JAERI-M
8595

PROPAGATION AND ABSORPTION OF THE FAST MAGNETOSONIC WAVE NEAR A TWO-ION HYBRID RESONANCE LAYER

November 1979

S. IIZUKA*, K. ODAJIMA, H. KIMURA, S. SENGOKU
T. SUGIE, K. TAKAHASHI, T. YAMAUCHI, K. KUMAGAI
T. KAWAKAMI, H. TAKEUCHI, H. MATSUMOTO,
T. MATSUDA K. OHASA, M. NAGAMI, S. YAMAMOTO,
T. NAGASHIMA, H. MAEDA, and Y. SHIMOMURA

日本原子力研究所
Japan Atomic Energy Research Institute

JAERI-M 8595

Propagation and Absorption of the Fast Magnetosonic Wave near a Two-ion Hybrid Resonance Layer

Satoru IIZUKA*, Kazuo ODAJIMA, Haruyuki KIMURA, Seio SENGOKU, Tatsuo SUGIE, Koki TAKAHASHI, Toshihiko YAMAUCHI, Katsuaki KUMAGAI, Tomohide KAWAKAMI, Hiroshi TAKEUCHI, Hiroshi MATSUMOTO, Toshiaki MATSUDA, Kazumi OHASA, Masayuki NAGAMI, Shin YAMAMOTO, Takashi NAGASHIMA, Hikosuke MAEDA and Yasuo SHIMOMURA

Division of Thermonuclear Fusion Research,
Tokai Research Establishment, JAERI

(Received November 9, 1979)

The experimental results of DIVA ICRF heating in a plasma consisting of the deuterium and the minority hydrogen ions were compared with the mode conversion theory including tunneling, reflection and absorption of the fast magnetosonic wave near a two-ion hybrid resonance layer.

Wave length and damping length of the wave propagating in the toroidal direction were measured directly from phase shift and amplitude of the excited wave detected by magnetic probes. Effective ion heating occurred at the optimum values of plasma parameters such as hydrogen to deuterium density ratio and strength of toroidal magnetic field, and in this case the damping length along the toroidal direction became a minimum. These results were consistent with the mode conversion theory. In the optimum case, the ion temperature with net rf power about 120 - 140 kW was increased spectacularly about three times from that without rf power, and it became larger than the electron temperature in the whole plasma column.

Keywords; ICRF Heating, Two-ion Hybrid Resonance, Mode Conversion, Fast Magnetosonic Wave, Wave Length, Damping Length, Ion Temperature, DIVA Tokamac

---

*) Special Research Student, Tohoku University, Sendai, Japan

JAERI－M 8595

2イオン混成共鳴層近傍における速進磁気流体波の伝搬および吸収

日本原子力研究所東海研究所核融合研究部
飯塚　哲*・小田島和男・木村晴行・仙石盛夫・
杉江達夫・高橋興起・山内俊彦・熊谷勝昭・
河上知秀・竹内　浩・松本　宏・松田俊明・大麻和美・
永見正幸・山本　新・永島　孝・前田彦祐・下村安夫・

（1979年11月9日受理）

DIVAで行われた小量のH_2を含むD_2プラズマ中のICRF加熱実験の結果と，2イオン混成共鳴層における磁気流体波（速進波）の透過，反射および吸収を含むモード変換理論との比較を行う。

磁気プローブによって，トロイダル方向に伝搬する速進波の波長および減衰長が直接測定された。H_2とD_2の密度比やトロイダル磁場の強さ等のプラズマパラメータを最適値に選ぶことによって，効率よいイオン加熱が起こり，そのときトロイダル方向の速進波の減衰長が最小となることが明らかになった。速進波の波長，減衰長およびイオン温度の上昇等の諸結果は，モード変換理論の諸結果と矛盾しない。120～140 kWの高周波パワーを印加すると，最適時にはイオン温度が非常に上昇して，印加しないときの3倍に達し，プラズマ全空間にわたってイオン温度が電子温度よりも高いプラズマを作ることに成功した。

*）核融合特別研究生　東北大学工学部

Contents

目　　次

1. Introduction

A plasma consisting of two or more ion species in a static magnetic field has new interesting properties in the vicinity of their fundamental ion cyclotron frequency region[1]. When the plasma density is increased, two gyrated ion species are strongly coupled with each other to produce a two-ion hybrid resonance in the intermediate frequency region of their fundamental ion cyclotron frequencies, which value is determined by the density ratio of two ions.

Concerning the fast magnetosonic auxiliary wave heating in the deuterium plasma with minority hydrogen[2]~[7], the damping decrement of the excited wave was too large to be explained only by the normal second harmonic cyclotron damping. The reason of these incredible increment of the wave damping was clarified by the several experiments performed in TFR[5], and TM1[3]. The presence of hydrogen as a small amount of impurities produces two-ion hybrid resonance near the cyclotron resonance layer at which the fast magnetosonic wave is locally converted to a slow electrostatic ion Bernstein mode whose power is consequently transferred to the plasma particles by ion cyclotron damping and electron Landau damping[8]~[12]. Recently, the detailed calculation for the condition of the mode conversion and the damping length under the various values of the hydrogen to deuterium density ratio has been reported[15].

Tunneling and absorption of the incident wave power near the resonance layer was first discussed by Budden[13]. Tunneling and reflection coefficients were obtained by using a second order wave equation containing a zero and a pole of wave number, which indicate that the absorption takes place at the singular turning layer. Ngan et al.[14] investigated the mode conversion from the fast magnetosonic wave to the ion Bernstein wave in a warm, collisionless, toroidal plasma and the tunneling and the reflection coefficient of the fast magnetosonic wave were calculated theoretically.

Several experimental results were tried to be explained by these mode conversion theory[8][9]. The experimental results, however, were not sufficient to prove the mode conversion theory because the dependences on the parameters such as hydrogen concentration, wave number and damping length were not investigated experimentally.

Here, we discuss the comparison between the mode conversion theory obtained by Ngan et al. and the experimental results performed in DIVA ICRF heating in which plasma parameters have been surveyed for the

optimium ion heating by varing the hydrogen to deuterium density ratio and the toroidal magnetic field[16][17]. The presence of an optimium condition for efficient ion heating is well agreed with the theory.

In the next section, we discuss the mode conversion theory and in section 3 the experimental and the theoretical results are compared. Conclusions are described in section 4.

2. Theoretical Consideration

Theoretical analysis starts from clarifications of property of the dispersion relation of the fast magnetosonic wave including a thermal effect which is very important for the discussion of the mode conversion. Next, accessibility for the fast magnetosonic wave is calculated. In sub-section 3, tunneling, reflection and absorption of the fast magnetosonic wave are calculated by using a forth order wave equation. The damping length in the toroidal direction is also calculated in the last section.

2.1 Dispersion relation

We consider a collisionless and fully ionized toroidal plasma consisting of the deuterium and minority hydrogen immersed in a toroidal magnetic field directed in z. The major radius is directed in x whose origin is a center of the plasma column with radius a. The major radius is R. The dispersion relation in this system is described approximately as follows.

$$F = \begin{vmatrix} K_{xx} - n_{/\!/}^2, & iK_{xy}, & n_{/\!/}n_{\perp} \\ -iK_{xy}, & K_{yy} - n_{/\!/}^2 - n_{\perp}^2, & 0 \\ n_{/\!/}n_{\perp}, & 0 & , K_{zz} - n_{\perp}^2 \end{vmatrix} = 0 \qquad (1)$$

where K_{ij} is components of the dielectric tensor.

The approximate forms of the components of the dielectric tensor for long wave length region where $k_{\perp}\rho_i < 1$ are obtained by an expansion of the coefficient $I_n(\lambda)\, e^{-\lambda}$ in a series λ, where $\lambda = k_{\perp}^2\rho_i^2/2$. Then the first order equations are as follows.

optimium ion heating by varing the hydrogen to deuterium density ratio and the toroidal magnetic field[16][17]. The presence of an optimium condition for efficient ion heating is well agreed with the theory.

In the next section, we discuss the mode conversion theory and in section 3 the experimental and the theoretical results are compared. Conclusions are described in section 4.

2. Theoretical Consideration

Theoretical analysis starts from clarifications of property of the dispersion relation of the fast magnetosonic wave including a thermal effect which is very important for the discussion of the mode conversion. Next, accessibility for the fast magnetosonic wave is calculated. In sub-section 3, tunneling, reflection and absorption of the fast magnetosonic wave are calculated by using a forth order wave equation. The damping length in the toroidal direction is also calculated in the last section.

2.1 Dispersion relation

We consider a collisionless and fully ionized toroidal plasma consisting of the deuterium and minority hydrogen immersed in a toroidal magnetic field directed in z. The major radius is directed in x whose origin is a center of the plasma column with radius a. The major radius is R. The dispersion relation in this system is described approximately as follows.

$$F = \begin{vmatrix} K_{xx} - n_{/\!/}^2, & iK_{xy}, & n_{/\!/}n_{\perp} \\ -iK_{xy}, & K_{yy} - n_{/\!/}^2 - n_{\perp}^2, & 0 \\ n_{/\!/}n_{\perp}, & 0 & , K_{zz} - n_{\perp}^2 \end{vmatrix} = 0 \qquad (1)$$

where K_{ij} is components of the dielectric tensor.

The approximate forms of the components of the dielectric tensor for long wave length region where $k_{\perp}\rho_i < 1$ are obtained by an expansion of the coefficient $I_n(\lambda)\, e^{-\lambda}$ in a series λ, where $\lambda = k_{\perp}^2\rho_i^2/2$. Then the first order equations are as follows.

$$K_{xx} \simeq 1 - \frac{\omega_{pe}^2}{\omega^2-\omega_{ce}^2} - \frac{\omega_{PH}^2}{2\omega^2}\left[\left(\frac{\omega}{\omega+\omega_{CH}} - \frac{\omega}{k\,V_{TH}}Z_H\right)(1-\lambda_H)+\lambda_H\frac{2\omega^2}{\omega^2-4\omega_{CH}^2}\right]$$

$$- \frac{\omega_{PD}^2}{2\omega^2}\left[\frac{2\omega^2}{\omega^2-\omega_{CD}^2}(1-\lambda_D) + \lambda_D\left(\frac{\omega}{\omega+2\omega_{CD}} - \frac{\omega}{k\,V_{TD}}Z_D\right)\right]$$

$$K_{yy} \simeq 1 - \frac{\omega_{pe}^2}{\omega^2-\omega_{ce}^2} - \frac{\omega_{PH}^2}{2\omega^2}\left[\left(\frac{\omega}{\omega+\omega_{CH}} - \frac{\omega}{k\,V_{TH}}Z_H\right)(1-3\lambda_H)+\lambda_H\frac{2\omega^2}{\omega^2-4\omega_{CH}^2}\right]$$

$$- \frac{\omega_{PD}^2}{2\omega^2}\left[\frac{2\omega^2}{\omega^2-\omega_{CD}^2}(1-3\lambda_D) + \lambda_D\left(\frac{\omega}{\omega+2\omega_{CD}} - \frac{\omega}{k\,V_{TD}}Z_D\right)\right] \qquad (2)$$

$$K_{zz} \simeq 1 - \frac{\omega_{PH}^2}{\omega^2} - \frac{\omega_{PD}^2}{\omega^2} + \frac{2\omega_{pe}^2}{k^2V_{Te}^2}\left(1 + \frac{\omega}{k\,V_{Te}}Z_e\right)$$

$$K_{xy} \simeq -\frac{\omega_{pe}^2}{\omega^2-\omega_{ce}^2}\frac{\omega_{ce}}{\omega} - \frac{\omega_{PH}^2}{2\omega^2}\left[\left(\frac{\omega}{\omega+\omega_{CH}} + \frac{\omega}{k\,V_{TH}}Z_H\right)(1-2\lambda_H)-\lambda_H\frac{4\omega\,\omega_{CH}}{\omega^2-4\omega_{CH}^2}\right]$$

$$- \frac{\omega_{PD}^2}{2\omega^2}\left[-\frac{2\omega\,\omega_{CD}}{\omega^2-\omega_{CD}^2}(1-2\lambda_D) + \lambda_D\left(\frac{\omega}{\omega+2\omega_{CD}} + \frac{\omega}{k\,V_{TD}}Z_D\right)\right]$$

where $n = \frac{kc}{\omega}$, $k_\perp^2 = k_x^2+k_y^2$, $k_{/\!/} = k_z$, and ω_c, ω_p, V_T are the cyclotron frequency, plasma frequency and thermal velocity, respectively. Z is a plasma dispersion function. Here, we discuss only a case $k_y = 0$.

The dispersion relation of the fast magnetosonic wave and the electrostatic ion Bernstein wave in which $\tilde{E}_x$, $\tilde{E}_y \gg E_z$ is approximately obtained from eq.(1) as follows,

$$F \simeq (K_{xx}-n_{/\!/}^2)(K_{yy}-n_{/\!/}^2-n_\perp^2) - K_{xy}^2 = 0 \ . \qquad (3)$$

The typical ω-k_x diagram with parameter of the density ratio n_H/n_0 is shown in Fig.1, where n_0 is an electron density. Frequencies and wave numbers are normalized by the fundamental hydrogen cyclotron frequency and by the wave length of the light in a vacuum, respectively. When the plasma contains a small amount of hydrogen, the wave dispersion relation is modified in the vicinity of the fundamental cyclotron frequency of the hydrogen. Here, the detailed explanation is devoted to

only the case of $n_H/n_0 = 0.1$. The branch A and B are the modes of the fast magnetosonic wave with the Alfvén phase velocity $\omega/k \simeq V_A$. The branch C approaches to two-ion cut off ($\omega/k_x \to \infty$) at $\omega = \omega_{cut}$, and the branch D approaches to two-ion hybrid resonance ($\omega/k_x \to 0$) at $\omega = \omega_{Res}$ in the cold approximation. Near the two-ion hybrid resonance, the effects of the finite Larmour radius appear, because that the perpendicular wave length approaches to an order of the ion Larmour radius, so that the cold approximate dispersion relation is not correct in such a region. The branch D is deformed to the branch E due to these effects. The branch E is corresponding to the electrostatic ion Bernstein wave which propagates in the perpendicular direction to the magnetic field. The branch F is also produced by the coupling of fast magnetosonic wave and ion Bernstein wave, where the square roots of the wave number becomes complex indicating an occurrence of the damping and the spontaneous excitation as a reflection.

So, we can see that the fast magnetosonic wave is converted to the electrostatic ion Bernstein wave near the two-ion hybrid resonance layer.

2.2 Accessibility condition

To make the mode conversion layer in the plasma column, we discuss the cold dispersion relation in the limit $\lambda \to 0$ in eq.(1). These approximation is correct in the cut off layer but is slightly modified in the two-ion hybrid resonance layer. In Fig.2, the two-ion hybrid resonance condition in ω_{pe}^2-ω_{CH} plane with the parameter n_H/n_0 and k_{zc}/ω_{CH} is shown as the curve S. The two-ion cut off condition, and the cut off condition of the fast magnetosonic wave are shown as the curve L and R, respectively. The curves S, L and R are obtained by the following equations.

$$S = K_{xx} - n_{//}^2 = 1 - \sum_j \frac{\omega_{pj}^2}{\omega^2-\omega_{cj}} - n_{//}^2 = 0$$

$$L = K_{xx} - K_{xy} - n_{//}^2 = 1 - \sum_j \frac{\omega_{pj}^2}{(\omega-\omega_{cj})\omega} - n_{//}^2 = 0 \qquad (4)$$

$$R = K_{xx} + K_{xy} - n_{//}^2 = 1 - \sum_j \frac{\omega_{pj}^2}{(\omega+\omega_{cj})\omega} - n_{//}^2 = 0$$

In the case of $n_H/n_0 = 0.1$ and $k_z c/\omega_{CH} = 3.2$, for example, the sign of the square perpendicular wave number k_x is changed reciprocally around the approximate intersection point P of the curve S, L and R. Upper the half plane of the curve R, only a narrow shaded region can be an evanescent region of the fast magnetosonic wave. The other region is a propagating region. Under the half plane of the curve R, only a narrow shaded region can be a propagating region and the other region is an evanescent region of the fast magnetosonic wave. These results conclude that when the parallel wave number is fixed, the plasma density must be sufficiently high enough to produce a two-ion hybrid resonance and a two-ion cut off in the center of the plasma column. Or if the plasma density is fixed, we must select the parallel wave number for the propagation to the mode conversion layer.

The two-ion hybrid resonance layer and the cut off layer in the plasma cross section is shown in Fig.3 under the condition that the plasma density and the toroidal magnetic field are changed as follows,

$$n_0(x)/n_0(0) = 1 - x^2$$
$$B_T(x)/B_T(0) = 1/(1+\delta x) \tag{5}$$

were $\delta = a/R$, $x = x/a$. The out region of the circle R except a narrow region surrounded by the curve S and L are a evanescent region for the fast magnetosonic wave. When the plasma density is decreased, the evanescent region becomes large, so the excited wave power does not sufficiently flow into the mode conversion layer.

Next, we find the accessibility condition of the fast magnetosonic wave using a cold plasma model. This condition can be obtained by the condition that the density at the point P must be smaller than that of the plasma center, whether it is included in the plasma or not, because that the density of the cut off curve R scarcely depends on the strength of the magnetic field.

By equating the curve L and R, the strength of the magnetic field at the point P in Fig.2 is easily obtained as follows,

$$\frac{\omega_{CH}^2}{\omega_{rf}^2} = \frac{1}{1 - \frac{3}{4}\varepsilon_H} \tag{6}$$

where $\varepsilon_H = n_H/n_0$.
Substituting eq.(6) into the two-ion hybrid resonance condition S = 0 in eq.(4), the electron plasma frequency at the point P is obtained.

$$\frac{\omega_{pe}^2}{\omega_{rf}^2} = \frac{3}{2}\frac{m_i}{m_e}(n_{//}^2 - 1)(1 - \frac{3}{4}\varepsilon_H)^{-1} \tag{7}$$

Then, we can obtain the accessibility condition as follows,

$$n_{//}^2 < 1 + \frac{2}{3}(1 - \frac{3}{4}\varepsilon_H)\left.\frac{\omega_{pe}^2}{\omega_{CH}\omega_{ce}}\right|_{n_{0,max}} \tag{8}$$

When the value n_z is increased, parallel phase velocity approaches to electron thermal velocity at the plasma periphery, so the wave energy is absorbed by electron Landau damping before the absorption at a plasma center. These phenomena cause unexpected periphery electron heating or the unnecessary excitation of the electrostatic wave. So we must limit the initial phase velocity to be smaller than the electron thermal velocity whose condition is

$$n_z < \frac{c}{V_{Te}} . \tag{9}$$

The wave which satisfies the condition(8) and (9) can propagate to a plasma center. Next problem is how much power of the incident wave are converted to the electrostatic ion Bernstein mode. We discuss this problem in the next sub-section.

2.3 Tunneling, reflection and absorption near the mode conversion layer

Ion Bernstein wave converted from the fast magnetosonic wave is dissipated by the cyclotron damping and Landau damping to heat a plasma. Although the detailed damping mechanisms for each particles are varied by the plasma parameters, the wave power of the ion Bernstein wave would be consequently absorbed by the plasma particles.

Therefore, we can estimate the power absorption of the plasma as the power converted to the ion Bernstein wave. When the plasma is inhomogeneous, the parameters such as ω_c, ω_p are changed at the different point. In this case, we must go back to the full wave equation to

understand the whole properties of the plasma.

The approximate wave equation including the fast magnetosonic wave and also the ion Bernstein wave are already obtained as in the following form[14].

$$\frac{\partial^4 \tilde{E}}{\partial \zeta^4} + \lambda^2 \zeta \frac{\partial^2 \tilde{E}}{\partial \zeta^2} + (\lambda^2 \zeta + \gamma)\, \tilde{E} = 0 \tag{10}$$

This forth order wave equation is deformed into the simple second order wave equations discussed by Budden under the assumption that $\lambda^2 \to \infty$ and $\gamma \to \infty$ with the constant $\frac{\gamma}{\lambda^2}$. Then,

$$\frac{\partial^2 \tilde{E}}{\partial \zeta^2} + \left(1 + \frac{\eta_0}{\zeta}\right) \tilde{E} = 0 \tag{11}$$

and $$\frac{\partial^4 \tilde{E}}{\partial \zeta^4} + \lambda^2 \zeta \frac{\partial^2 \tilde{E}}{\partial \zeta^2} = 0$$

where $\eta_0 = \gamma/\lambda^2$.

So physically, the second and the third term describe the fast magnetosonic wave equation near the pole, and the first term explains how much energy of the incident wave carried away by the ion Bernstein wave. We discuss the power absorption by using a full wave equation (10).

The local dielectric tensor given by eq.(2) must be expanded around the two-ion hybrid resonance layer at $x = x_{res}$ with the small variable $\zeta = x - x_{res}$. Then, we obtain the first order approximate equations in the case of $n_H/n_0 \ll 1$.

$$K_{xx} \simeq \frac{8}{9}\frac{\delta\alpha M}{\varepsilon_H'}\left(1 - \frac{3}{4}\varepsilon_H'\right)\zeta + \frac{\alpha M W^2}{3\varepsilon_H'}\left(1 - \frac{3}{2}\varepsilon_H'\right) K_x^2$$

$$K_{yy} \simeq K_{xx} \tag{12}$$

$$K_{xy} \simeq \frac{2\alpha M}{3\varepsilon_H'}\left(1 - \varepsilon_H'\right) - \frac{8}{9}\frac{\delta\alpha M}{\varepsilon_H'}\left(1 - \frac{3}{4}\varepsilon_H'\right)\zeta$$

where $W = \frac{V_{Te}}{C}\sqrt{M\frac{T_e}{T_i}}$, $M = \frac{m_i}{m_e}$, $\alpha = \frac{\omega_{pe}^2}{\omega_{ce}^2}$,

$$\varepsilon_H' = \varepsilon_H/(1 + \frac{3n_{//}^2}{2\alpha M})$$

Using these results, the wave equation is reduced to the form of eq.(10). The value λ^2 and γ are given as,

$$\lambda^2 \simeq \frac{\sqrt{3}\ \delta}{W^2 g(\alpha M)^{3/2}}$$

$$\gamma \simeq \frac{3\varepsilon_H'}{4\alpha M W^2} \qquad (13)$$

where $g = \frac{\omega_{CH}{}^a}{C}$.

Then, we get the absorption parameter η for the power absorption.

$$\eta = \frac{\pi(\alpha M)^{3/2}\ W^2 g}{2\sqrt{3}\ \delta}(1 + \frac{3\varepsilon_H'}{4\alpha M W^2}) \ . \qquad (14)$$

The tunneling coefficient C_T and the reflection coefficient C_R are slightly different whether the fast magnetosonic wave is launched from the higher magnetic field side or the lower magnetic field side. For the incident wave from the lower magnetic field side,

$$C_T = e^{-\eta}$$

$$C_R = 1 - e^{-2\eta} \qquad (15)$$

and for the incident wave from the higher magnetic field side,

$$C_T = e^{-\eta}$$

$$C_R = 0 \qquad (16)$$

These coefficients have following physical meanings. When the wave with amplitude $e^{j\zeta}$ is launched from the lower magnetic field side which is sufficiently apart from the mode conversion layer, the amplitude of the reflecting wave and the tunneling wave are reduced like $(1-e^{-2\eta})e^{j\zeta}$ and $e^{-\eta}e^{j\zeta}$, respectively. So the power ratio of the reflecting wave and the tunneling wave to the incident wave are $(1-e^{-2\eta})^2$ and $e^{-2\eta}$, respectively. The total power converted to the ion Bernstein wave for the incident wave from the lower magnetic field side,

$$P_L = e^{-2\eta}(1-e^{-2\eta}) \quad , \tag{17}$$

and for the incident wave from the higher magnetic field side,

$$P_H = 1 - e^{-2\eta} \quad . \tag{18}$$

when $\eta \gg 1$, then $P_L \to 0$ and $P_H \to 1$, which indicate the perfect reflection and absorption are taken place, respectively. The dependence of P_L and P_H on the value η are shown in Fig.4. For the lower magnetic field side excitation, the most efficient power absorption occures at $\eta \simeq 0.35$ with $P_L \simeq 0.23$. For the higher magnetic field side excitation, large η is necessary for the efficient power absorption.

Next we must consider how the transmitted tunneling wave behaves. The transmitted wave must be damped somewhere. From the point of view of the wave propagation, the periphery of the plasma is an evanscent layer as shown in Fig.3, so a part of the fast magnetosonic wave may be reflected at this layer. Some part of wave energy, however, is transmitted through this layer to be carried to the wall of the device and consequently a part of wave power is reflected at the wall. From these considerations, a part of the transmitted power from the mode conversion to the periphery is again reflected back to the plasma center at the plasma periphery and the wall. The remains of the power are lost in such a region. Here, we define the effective reflection coefficient at the periphery as follows,

$$\xi = \frac{P_{\text{reflection}}}{P_{\text{out}}} \tag{19}$$

where P_{out} is an outgoing power from the plasma center.
The model of these systems is shown in Fig.5. This reflected wave power again comes to the mode conversion layer and a part of its energy is converted to the ion Bernstein mode. These absorption, transmission and reflection runs so many times in the x direction untill the wave power is heavily damped during the propagation along the toroidal direction.

The total absorption power after infinite repetition is obtained by summing up of the infinite geometric progression. For the incident wave from the lower magnetic field side,

$$P_{L.T} = \frac{a_0 + a_1 b_0 \xi}{1 - a_2 \xi - a_1 b_1 \xi^2} \tag{20}$$

and for the incident wave from the higher magnetic field side,

$$P_{H.T} = \frac{b_0 + (a_0 b_1 - a_2 b_0)\xi}{1 - a_2 - a_1 b_1 \xi^2} \tag{21}$$

where $a_0 = e^{-2\eta}(1-e^{-2\eta})$

$a_1 = e^{-2\eta}$

$a_2 = (1-e^{-2\eta})^2$

$b_0 = 1 - e^{-2\eta}$

$b_1 = e^{-2\eta}$

The value of $P_{L.T}$ and $P_{H.T}$ depending on η with parameter ξ is shown in Fig.6. When ξ is approached to unity, the incident wave power is perfectly absorbed.

2.4 Toroidal damping length

The damping length of the incident wave in the toroidal z direction is determined by the absorption rate of the fast magnetosonic wave in x direction. The characteristic distance d is obtained by using an average radial wave number $\bar{k}_x$ of the fast magnetosonic wave.

$$d = 4\frac{\bar{k}_x}{k_z} a \tag{22}$$

When the wave is launched from the lower magnetic field side, it is easily obtained from Fig.5 that the wave power after traveling the distance d in the region far from the exciting point is reduced by the factor $\xi^2(a_2^2+2a_1b_1)$. So we can calculate the power damping length at which the wave power becomes e^{-1} compared with the initial wave power as follows,

$$\frac{\lambda_d}{d} = \frac{-1}{\ell n[\xi^2(a_2^2+2a_1b_1)]} \tag{23}$$

The damping length normalized by the characteristic distance d with the parameter ξ is shown in Fig.7 and the wave power variation along the z direction with the parameter η is shown in Fig.8. The most heavy wave damping occurs at $\eta \simeq 0.5$ at which the mode conversion occurs effectively as shown in Fig.6. The damping length is increased as the reflection coefficient ξ is much increased.

In conclusion, the parameter η is the most important factor for the effective plasma heating. As the parameter η is dependent on the plasma density, strength of the magnetic field, plasma temperature, parallel wave number and also the density ratio n_H/n_0, the plasma parameters must be determined so as to select $\eta \simeq 0.5$ for the incident wave from the lower magnetic field side and $\eta \geq 0.5$ for the incident wave from the higher magnetic field side.

3. Experimental Apparatus

Fast magnetosonic wave heating are performed in JFT-2a (DIVA) tokamak[16] with a divertor. The major radius R = 60 cm and the minor radius a = 10 cm. The rf frequency $\omega_{rf}/2\pi$ = 25 MHz is equal to the fundamental ion cyclotron frequency of the hydrogen $\omega_{CH}/2\pi$ and also is equal to the second harmonic ion cyclotron frequency of the deuterium $\omega_{CD}/2\pi$ when the toroidal magnetic field B_T is 16.5 kG. The maximum of the rf power is about 200 kW. The generator system is shown in Fig.9.

A 10-channel charge exchange neutral particle energy analyzer is used for the measurement of the perpendicular ion temperature. The amplitude of the fast magnetosonic wave is measured with six magnetic probes which detect azimuthal component of the magnetic field fluctuations. These probes P_1, P_2, P_3, P_4, P_5, P_6 are placed at 0°, 90°, 180°, 35°, 45°, 55° from the antenna position in toroidal direction, respectively, as shown in Fig.11(a). These probes are made of one turn cupper

When the wave is launched from the lower magnetic field side, it is easily obtained from Fig.5 that the wave power after traveling the distance d in the region far from the exciting point is reduced by the factor $\xi^2(a_2^2+2a_1b_1)$. So we can calculate the power damping length at which the wave power becomes e^{-1} compared with the initial wave power as follows,

$$\frac{\lambda_d}{d} = \frac{-1}{\ell n[\xi^2(a_2^2+2a_1b_1)]} \tag{23}$$

The damping length normalized by the characteristic distance d with the parameter ξ is shown in Fig.7 and the wave power variation along the z direction with the parameter η is shown in Fig.8. The most heavy wave damping occurs at $\eta \simeq 0.5$ at which the mode conversion occurs effectively as shown in Fig.6. The damping length is increased as the reflection coefficient ξ is much increased.

In conclusion, the parameter η is the most important factor for the effective plasma heating. As the parameter η is dependent on the plasma density, strength of the magnetic field, plasma temperature, parallel wave number and also the density ratio n_H/n_0, the plasma parameters must be determined so as to select $\eta \simeq 0.5$ for the incident wave from the lower magnetic field side and $\eta \gtrsim 0.5$ for the incident wave from the higher magnetic field side.

3. Experimental Apparatus

Fast magnetosonic wave heating are performed in JFT-2a (DIVA) tokamak[16] with a divertor. The major radius R = 60 cm and the minor radius a = 10 cm. The rf frequency $\omega_{rf}/2\pi$ = 25 MHz is equal to the fundamental ion cyclotron frequency of the hydrogen $\omega_{CH}/2\pi$ and also is equal to the second harmonic ion cyclotron frequency of the deuterium $\omega_{CD}/2\pi$ when the toroidal magnetic field B_T is 16.5 kG. The maximum of the rf power is about 200 kW. The generator system is shown in Fig.9.

A 10-channel charge exchange neutral particle energy analyzer is used for the measurement of the perpendicular ion temperature. The amplitude of the fast magnetosonic wave is measured with six magnetic probes which detect azimuthal component of the magnetic field fluctuations. These probes P_1, P_2, P_3, P_4, P_5, P_6 are placed at 0°, 90°, 180°, 35°, 45°, 55° from the antenna position in toroidal direction, respectively, as shown in Fig.11(a). These probes are made of one turn cupper

wire with diameter 5 mm and are shielded by using a co-axial cable to prevent electrostatic coupling. The power of the wave is also measured by frequency spectrum analyzer.

The density ratio n_H/n_0 is measured by the monocrometer. The value n_H/n_0 can be varied over the range of 2~40 % by controlling the amount of injected hydrogen gas.

The typical plasma parameters are as follows. Toroidal magnetic field B_T is 18 kG, electron and ion temperature at the plasma center are 300 eV and 160 eV, respectively, line average electron density $\bar{n}_e$ is 3.5×10^{13} cm^{-3}, one turn loop voltage V_L is about 2.5 V, plasma current I_P is 30 KA, and effective charge number Z_{eff} is almost unity.

4. Experimental results

The time evolutions of the plasma current I_P, one turn voltage V_L and the electron density n_e are shown in Fig.10(a) and (b), respectively, with B_T = 17.5 kG and $n_H/n_0 \simeq 8$ %. The rf power is applied from 9 ms to 12 ms. The plasma parameters are almost constant during the rf pulse. The time evolution of the ion temperature measured by the charge exchange neutral analyzer is shown in Fig.10(c). Ion temperature increases from 160 eV up to 430 eV, when the rf power including the circuit loss is about 180 kW. This value is about three times larger than the basic ion temperature, and exceeds the electron temperature of the plasma center. It should be noted that at least 80 % of the rf power without circuit loss is absorbed by ions at the central region of the plasma. The efficiency is extremely higher than the other rf heating.

4.1 Toroidal wave length

To investigate the heating mechanism of these effective ion heating described above, first of all it is important to know how the excited fast magnetosonic wave propagates in the plasma. These informations are obtained by the measurement of the six magnetic probes placed at the different positions in toroidal direction as shown in Fig.11(a). The typical power spectrum of the fast magnetosonic wave measured by P_1, P_2 and P_3 are shown in Fig.11(b). Along the toroidal direction wave amplitude is decreased. Higher harmonics are observed probably due to the distortion of the wave form of the generator, but those powers are less 10 dB than that of the fundamental wave power. The phase and the amplitude of the wave detected by the probe P_4, P_5 and P_6 are shown in

wire with diameter 5 mm and are shielded by using a co-axial cable to prevent electrostatic coupling. The power of the wave is also measured by frequency spectrum analyzer.

The density ratio n_H/n_0 is measured by the monocrometer. The value n_H/n_0 can be varied over the range of 2~40 % by controlling the amount of injected hydrogen gas.

The typical plasma parameters are as follows. Toroidal magnetic field B_T is 18 kG, electron and ion temperature at the plasma center are 300 eV and 160 eV, respectively, line average electron density $\bar{n}_e$ is 3.5×10^{13} cm^{-3}, one turn loop voltage V_L is about 2.5 V, plasma current I_P is 30 KA, and effective charge number Z_{eff} is almost unity.

4. Experimental results

The time evolutions of the plasma current I_P, one turn voltage V_L and the electron density n_e are shown in Fig.10(a) and (b), respectively, with B_T = 17.5 kG and $n_H/n_0 \simeq 8$ %. The rf power is applied from 9 ms to 12 ms. The plasma parameters are almost constant during the rf pulse. The time evolution of the ion temperature measured by the charge exchange neutral analyzer is shown in Fig.10(c). Ion temperature increases from 160 eV up to 430 eV, when the rf power including the circuit loss is about 180 kW. This value is about three times larger than the basic ion temperature, and exceeds the electron temperature of the plasma center. It should be noted that at least 80 % of the rf power without circuit loss is absorbed by ions at the central region of the plasma. The efficiency is extremely higher than the other rf heating.

4.1 Toroidal wave length

To investigate the heating mechanism of these effective ion heating described above, first of all it is important to know how the excited fast magnetosonic wave propagates in the plasma. These informations are obtained by the measurement of the six magnetic probes placed at the different positions in toroidal direction as shown in Fig.11(a). The typical power spectrum of the fast magnetosonic wave measured by P_1, P_2 and P_3 are shown in Fig.11(b). Along the toroidal direction wave amplitude is decreased. Higher harmonics are observed probably due to the distortion of the wave form of the generator, but those powers are less 10 dB than that of the fundamental wave power. The phase and the amplitude of the wave detected by the probe P_4, P_5 and P_6 are shown in

Fig.12(a). Each probe is separated 10 degrees in the toroidal direction. The relative squared amplitude and the delay time normalized by the period of the wave along the toroidal angle are shown in Fig.12(b). From this figure, the excited wave is traveling in the toroidal direction with the wave length,

$$\lambda_z \simeq 42 \text{ cm} \quad , \tag{24}$$

which is corresponding to one ninth of the toroidal circumference. From this toroidal wave length, we can obtain the parallel phase velocity of the excited wave.

$$v_{ph.} = \frac{\omega_{rf}}{k_z} \simeq 1.0 \times 10^9 \quad (\text{cm/s}) \quad . \tag{25}$$

On the other hand, the Alfvén velocity is

$$V_A \simeq 7.2 \times 10^8 \quad (\text{cm/s}) \quad . \tag{26}$$

So the observed parallel phase velocity is the same order of the Alfvén velocity, which indicates that these detected waves should be fast magnetosonic waves. For the toroidal wave length, we must consider the accessibility condition whether this obtained wave length is reasonable or not. From eq.(8), when $\varepsilon_H = 0.08$,

$$\lambda_z > 30 \text{ cm} \quad . \tag{27}$$

The second condition given by eq.(9) for avoiding the direct coupling with the electron is also calculated as $T_e \simeq 300$ eV.

$$\lambda_z > 29 \text{ cm} \quad . \tag{28}$$

The measured toroidal wave length given by eq.(24) satisfies both conditions eq.(27) and eq.(28), which shows that the excited fast magnetosonic wave can be propagated to the mode conversion layer.

4.2 Toroidal damping length

Next we can determine a power damping length when $\varepsilon_H \simeq 8$ % and 20 % from the measured amplitude. In Fig.13, the amplitude dependence on the toroidal angles are shown. When $n_H/n_0 \simeq 8$ %, the toroidal damping length at which the initial wave power is reduced to e^{-1} can be obtained as the toroidal angle whose value is about 43 degrees. The corresponding toroidal damping length is about,

$$\lambda_d \simeq 45 \text{ cm} \quad , \tag{29}$$

which is comparable to the toroidal wave length.
And when $n_H/n_0 = 20$ %, as the toroidal damping angle is about 115 degrees, then

$$\lambda_d \simeq 120 \text{ cm} \quad . \tag{30}$$

Using the measured parallel wave length, the value η corresponding to the ratio n_H/n_0 can be calculated numerically by the full equation(10), which is shown in Fig.6 under the condition that the two-ion hybrid resonance layer is placed at the plasma center. When the ratio n_H/n_0 is 8 % and 20 %, the corresponding value η is 0.5 and 1.5, respectively. Here, we do not know the value ξ. The damping length normalized by the characteristic distance d is obtained numerically in Fig.7. In these results, when $\eta \simeq 0.5$, the damping length is not widely varied by the value ξ and is almost constant,

$$\lambda_d/d \simeq 1 \quad . \tag{31}$$

The experimental damping length given by eq.(29) normalized by the parallel wave length given by eq.(24) is,

$$\lambda_d/\lambda_z \simeq 1 \quad . \tag{32}$$

From above two results, we can decide the relation between the distance d and the wave length λ_z, then

$$d \simeq \lambda_z \simeq 42\text{~}45 \text{ cm}. \tag{33}$$

We can estimate the averaged perpendicular wave number $\bar{k}_x$ from eq.(22), that is $\bar{k}_x \simeq 0.16 \text{ cm}^{-1}$, which value is consistent with that obtained from the local dispersion relation of the fast magnetosonic wave.

4.3 Reflection coefficient ξ

Using the results described above, the reflection coefficient ξ at periphery is determined in the case of $n_H/n_0 = 8$ % and 20 %. The amplitude dependence on the toroidal angle with the parameter ξ calculated from eq.(23) is shown in Fig.13. The common value ξ which fit both cases of $n_H/n_0 \simeq 8$ % and 20 % is about

$$\xi \simeq 0.9 \quad . \tag{34}$$

4.4 Dependence on n_H/n_0

Varying the density ratio n_H/n_0 by controlling the injection of amount of hydrogen gas, we measure the increase of the ion temperature normalized by the incident net power as shown in Fig.14. The most effective ion heating occurs when $n_H/n_0 \simeq 5\text{~}10$ %. In this figure, the absorbed power, i.e. the power converted to the ion Bernstein wave is also presented with the parameter ξ. Experimental results and the calculated curve qualitatively agree with each other. The fitted curve to the experimental results is in the case of $\xi \simeq 0.8\text{~}0.9$ which is consistent with the result described above in eq.(34). When $\xi \simeq 0.9$ and $n_H/n_0 = 8$ %, the absorbed power is expected to be about 85 % of the incident wave power.

4.5 Dependence on B_T

Next, we must investigate how the power absorption is changed by the position of the mode conversion layer in a plasma column. Experimentally, these situations are realized by varying the toroidal magnetic field B_T.

First of all, we calculate the dependence η on B_T under the constant ratio $n_H/n_0 \simeq 8$ % and $\xi \simeq 0.9$. If the magnitude B_T is changed, the ion cyclotron layer and also the two-ion hybrid layer are shifted in the x direction. So the ratio α of the density, the strength of the toroidal

magnetic field at two-ion hybrid layer, the effective aspect ratio δ and also the plasma temperature W in eq.(14) are changed by B_T. Assuming the density profile and the magnetic field given in eq.(5), and also the paraboric plasma temperature dependences on x, the value η is obtained numerically from eq.(14) using a measured value k_z amd ξ, which is shown in Fig.15. The value η has a maximum when $B_T \simeq 18$ kG and is asymmetric against the geometric plasma center. The hydrogen cyclotron layer lies at the plasma center in the case of $B_T = 16.4$ kG. The maximum value η is about 0.46 which is nearly equal to the optimum value as known from Fig.6. The toroidal damping length and the total absorbed power are calculated from eq.(23) and eq.(20), respectively. The relative wave amplitude at the position $z = \lambda_z$ is also presented in Fig.15. From the above consideration, the most effective ion heating occurs when $B_T = 18$ kG and $n_H/n_0 \simeq 8$ %, and in this condition the wave amplitude will be heavily damped in the toroidal direction.

The wave amplitude detected by the magnetic probe P_3 with the various toroidal magnetic field is shown in Fig.16. The measured amplitude becomes minimum at $B_T = 18$ kG. The solid line is the relative amplitude calculated from the damping length at the position $z/\lambda_z = 4.5$. The curve agrees with the experimental results.

The relative increase of the ion temperature normalized by the incident net power against to B_T is shown in Fig.17. The solid line is an absorption coefficient calculated by eq.(20). When $B_T = 18$ kG, the increase of the ion temperature has a maximum, which is well agreed with the theoretical predictions.

5. Conclusions

The comparison was done between the experimental results obtained ICRF heating in DIVA and the mode conversion theory to investigate the heating mechanism of the plasma particles. The following results are clarified.

(1) The toroidal wave length measured by the magnetic probes satisfies the accessibility condition to make two-ion hybrid resonance layer in a plasma center. The toroidal phase velocity is an order of the Alfvén velocity and is larger than the electron thermal velocity.

(2) The toroidal power damping length measured by the magnetic probes can be explained by a model including an absorption due to the mode conversion near the two-ion hybrid resonance layer and a

magnetic field at two-ion hybrid layer, the effective aspect ratio δ and also the plasma temperature W in eq.(14) are changed by B_T. Assuming the density profile and the magnetic field given in eq.(5), and also the paraboric plasma temperature dependences on x, the value η is obtained numerically from eq.(14) using a measured value k_z amd ξ, which is shown in Fig.15. The value η has a maximum when $B_T \simeq 18$ kG and is asymmetric against the geometric plasma center. The hydrogen cyclotron layer lies at the plasma center in the case of $B_T = 16.4$ kG. The maximum value η is about 0.46 which is nearly equal to the optimum value as known from Fig.6. The toroidal damping length and the total absorbed power are calculated from eq.(23) and eq.(20), respectively. The relative wave amplitude at the position $z = \lambda_z$ is also presented in Fig.15. From the above consideration, the most effective ion heating occurs when $B_T = 18$ kG and $n_H/n_0 \simeq 8$ %, and in this condition the wave amplitude will be heavily damped in the toroidal direction.

The wave amplitude detected by the magnetic probe P_3 with the various toroidal magnetic field is shown in Fig.16. The measured amplitude becomes minimum at $B_T = 18$ kG. The solid line is the relative amplitude calculated from the damping length at the position $z/\lambda_z = 4.5$. The curve agrees with the experimental results.

The relative increase of the ion temperature normalized by the incident net power against to B_T is shown in Fig.17. The solid line is an absorption coefficient calculated by eq.(20). When $B_T = 18$ kG, the increase of the ion temperature has a maximum, which is well agreed with the theoretical predictions.

5. Conclusions

The comparison was done between the experimental results obtained ICRF heating in DIVA and the mode conversion theory to investigate the heating mechanism of the plasma particles. The following results are clarified.

(1) The toroidal wave length measured by the magnetic probes satisfies the accessibility condition to make two-ion hybrid resonance layer in a plasma center. The toroidal phase velocity is an order of the Alfvén velocity and is larger than the electron thermal velocity.

(2) The toroidal power damping length measured by the magnetic probes can be explained by a model including an absorption due to the mode conversion near the two-ion hybrid resonance layer and a

reflection at the plasma periphery with the effective power absorption coefficient ξ.

(3) From the measurement of the toroidal damping length and the toroidal wave number, we can estimate the value ξ being about 0.9, which value is consistent with the dependences on the ratio n_H/n_0 and the toroidal magnetic field B_T.

(4) When the density ratio n_H/n_0 is varied, the increase of the ion temperature has a maximum value at $n_H/n_0 \simeq 5\sim10$ % in the experiment. These phenomena are explained by the mode conversion theory as shown in Fig.14, which indicates that the efficiency of the mode conversion is changed by the ratio n_H/n_0. The total power absorbed by the plasma particles is about 85 % in the optimum case $n_H/n_0 \simeq 8$ %, that is, $\eta \simeq 0.5$ when $\xi \simeq 0.9$.

(5) The position of the mode conversion layer in the plasma is very important for the effective heating because that the plasma parameters are changed by its position. The maximum increase of the ion temperature is occurred at $B_T \simeq 18$ kG which is corresponding to the value about $\eta \simeq 0.5$. This result is also consistent with the mode conversion theory.

(6) For the efficient particle heating due to the mode conversion near the two-ion hybrid resonance layer, we must consider at least two points. First, we must select the value η to be optimum value about 0.5 when the incident wave is excited from the lower magnetic field side. On the other hand, the value η must be selected to be larger than 0.5 when the incident wave is excited from higher magnetic field side. Secondly, it is important to get the large value $\xi(\leq 1)$ by the improvement of the conditions of the plasma periphery and the wall.

So we can expect the large increase of plasma temperature with high efficiency in the ICRF heating experiments.

Acknowledgement

We would like to thank Dr. Y. Tanaka, Y. Obata and S. Mori for their continuous encouragement.

reflection at the plasma periphery with the effective power absorption coefficient ξ.

(3) From the measurement of the toroidal damping length and the toroidal wave number, we can estimate the value ξ being about 0.9, which value is consistent with the dependences on the ratio n_H/n_0 and the toroidal magnetic field B_T.

(4) When the density ratio n_H/n_0 is varied, the increase of the ion temperature has a maximum value at $n_H/n_0 \simeq 5\sim10$ % in the experiment. These phenomena are explained by the mode conversion theory as shown in Fig.14, which indicates that the efficiency of the mode conversion is changed by the ratio n_H/n_0. The total power absorbed by the plasma particles is about 85 % in the optimum case $n_H/n_0 \simeq 8$ %, that is, $\eta \simeq 0.5$ when $\xi \simeq 0.9$.

(5) The position of the mode conversion layer in the plasma is very important for the effective heating because that the plasma parameters are changed by its position. The maximum increase of the ion temperature is occurred at $B_T \simeq 18$ kG which is corresponding to the value about $\eta \simeq 0.5$. This result is also consistent with the mode conversion theory.

(6) For the efficient particle heating due to the mode conversion near the two-ion hybrid resonance layer, we must consider at least two points. First, we must select the value η to be optimum value about 0.5 when the incident wave is excited from the lower magnetic field side. On the other hand, the value η must be selected to be larger than 0.5 when the incident wave is excited from higher magnetic field side. Secondly, it is important to get the large value $\xi(\lesssim 1)$ by the improvement of the conditions of the plasma periphery and the wall.

So we can expect the large increase of plasma temperature with high efficiency in the ICRF heating experiments.

Acknowledgement

We would like to thank Dr. Y. Tanaka, Y. Obata and S. Mori for their continuous encouragement.

References

(1) S. Buchsbaum, Phys. Rev. Lett. 5, 495 (1960), Phys. Fluids 3, 418 (1960).

(2) J. Adam et al., 5th Conf. Plasma Phys. and Nucl. Fusion Res. (Tokyo 1974) II, 65, (1975).

(3) V. Vdvin et al., JETP Lett. 14, 149 (1971), 3rd Int. Meeting on Heating of Toroidal Plasma (Grenoble) II, 349 (1976).

(4) N. Ivanov et al., JETP Lett. 20, 39 (1974).

(5) TFR Group, 3rd Int. Meeting on Heating of Toroidal Plasma (Grenoble) I, 87 (1976), 6th Conf. Plasma Phys. and Nucl. Fusion Res. (Berchtesgaden 1976) III, 39 (1977).

(6) H. Kimura, K. Odajima, S. Sengoku, S. Iizuka, T. Sugie, et al., JAERI-M 8429 (1979).

(7) H. Takahashi et al., Phys. Rev. Lett. 39, 31 (1977).

(8) J. Jacquinot et al., Phys. Rev. Lett. 39, 88 (1977).

(9) D.G. Swanson, Phys. Rev. Lett. 36, 316 (1976).

(10) T.H. Stix, Nuclear Fusion 15, 737 (1975).

(11) A.M. Messian et al., Phys. Lett. 71A, 431 (1979).

(12) F.W. Perkins, Nuclear Fusion 176, 1197 (1977).

(13) K.G. Budden, Radio Waves in Ionosphere (Cambridge University, Cambridge, 1961).

(14) Y.C. Ngan et al., Phys. Fluids 20, 1920 (1977).

(15) J. Jacquinot, J. Proc. of Joint Varenna-Grenoble Int. Symp. on Heating in Toroidal Plasmas, Grenoble (1978).

(16) DIVA Group, Nuclear Fusion 18, 1619 (1978).

(17) H. Kimura, K. Odajima, S. Sengoku, K. Ohasa, T. Sugie, et al., to be published in Nucl. Fusion 20 (1980).

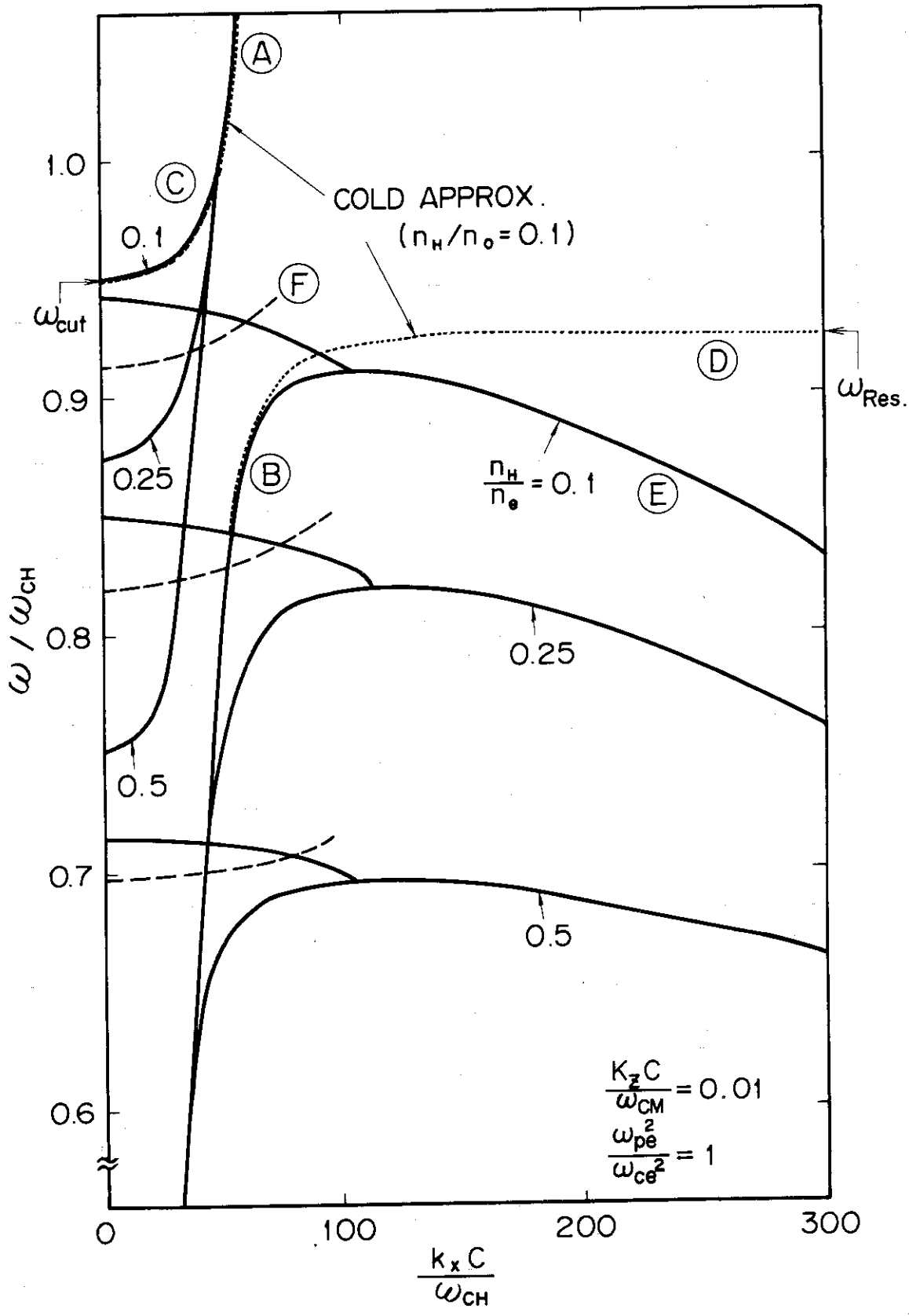

Fig. 1 Dispersion relation of the fast magnetosonic wave and ion Bernstein wave with parameter n_H/n_0.

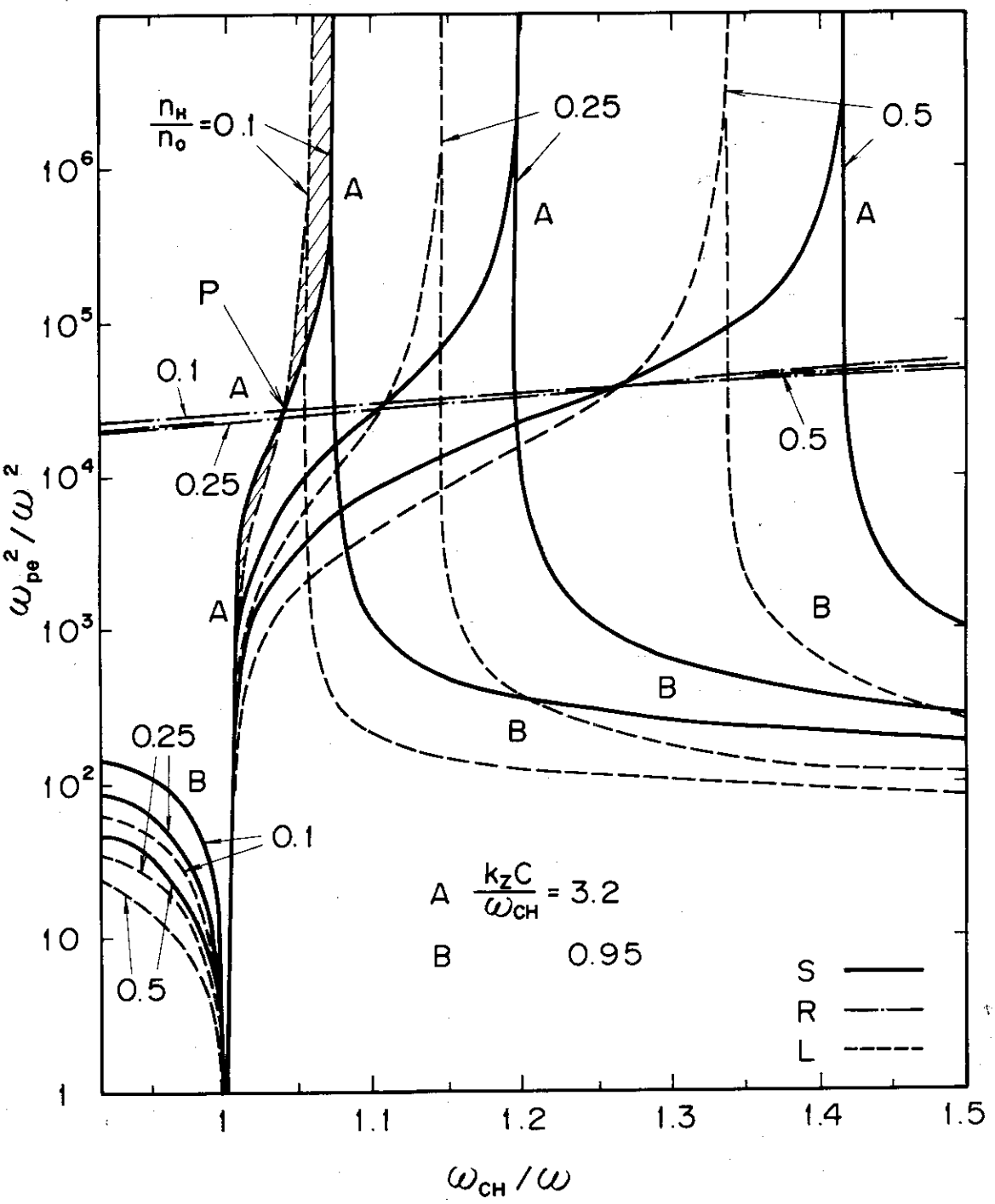

Fig. 2 Boundary of two-ion hybrid resonance and cut off in ω_{pe}^2-ω_{CH} plane with parameter n_H/n_0 and $k_z c/\omega_{CH}$.

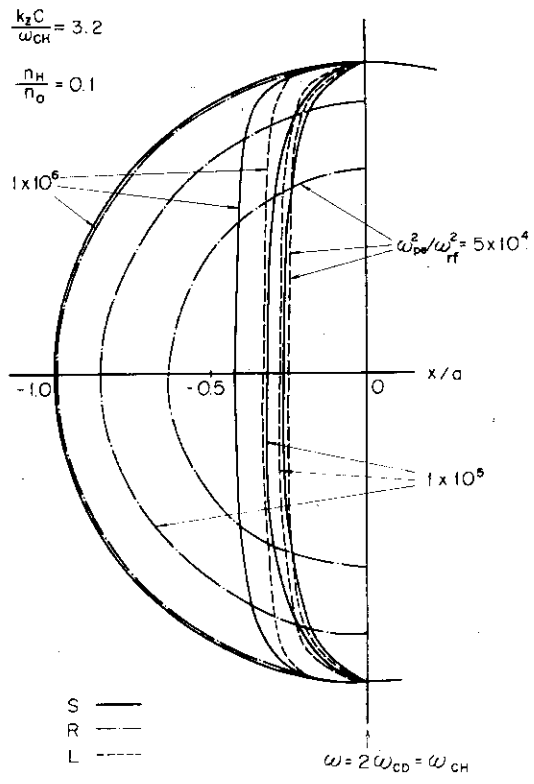

Fig. 3 Boundary of the two-ion hybrid resonance and cut off in the plasma cross section with parameter $\omega_{pe}^2/\omega_{rf}^2$.

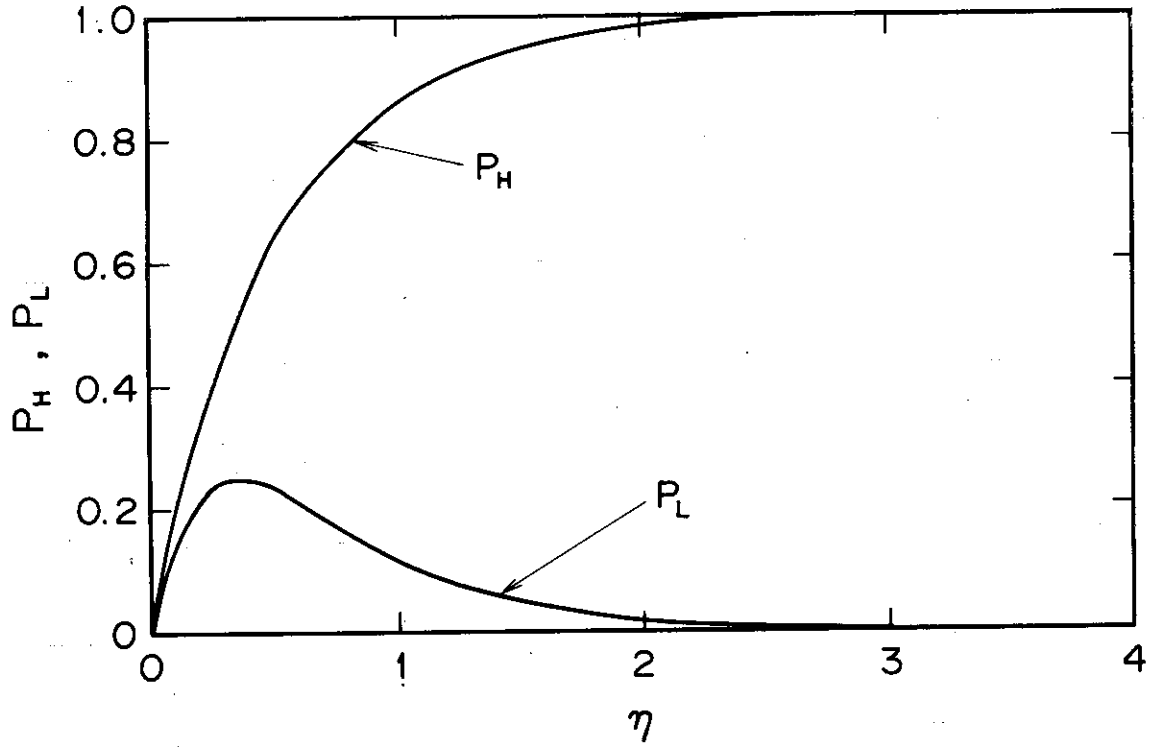

Fig. 4 Absorption power once through the mode conversion layer for the incident wave excited from the lower magnetic field side P_L and the higher magnetic field side P_H.

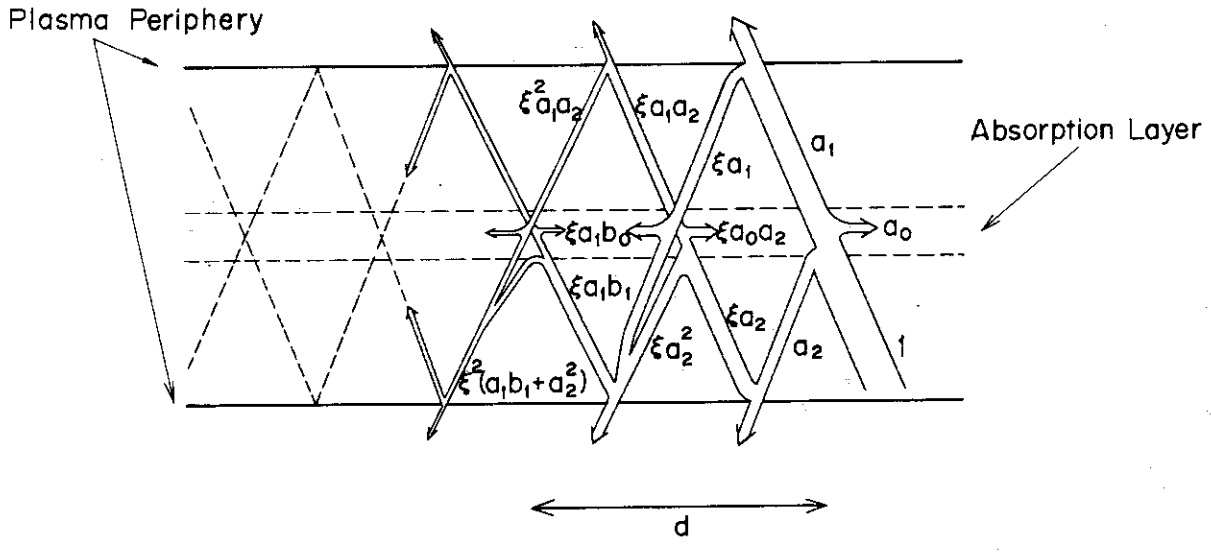

Fig. 5 Model of the energy flow in a plasma. The wave propagates and reflects so many times to be consequently absorbed by a plasma during toroidal propagation.

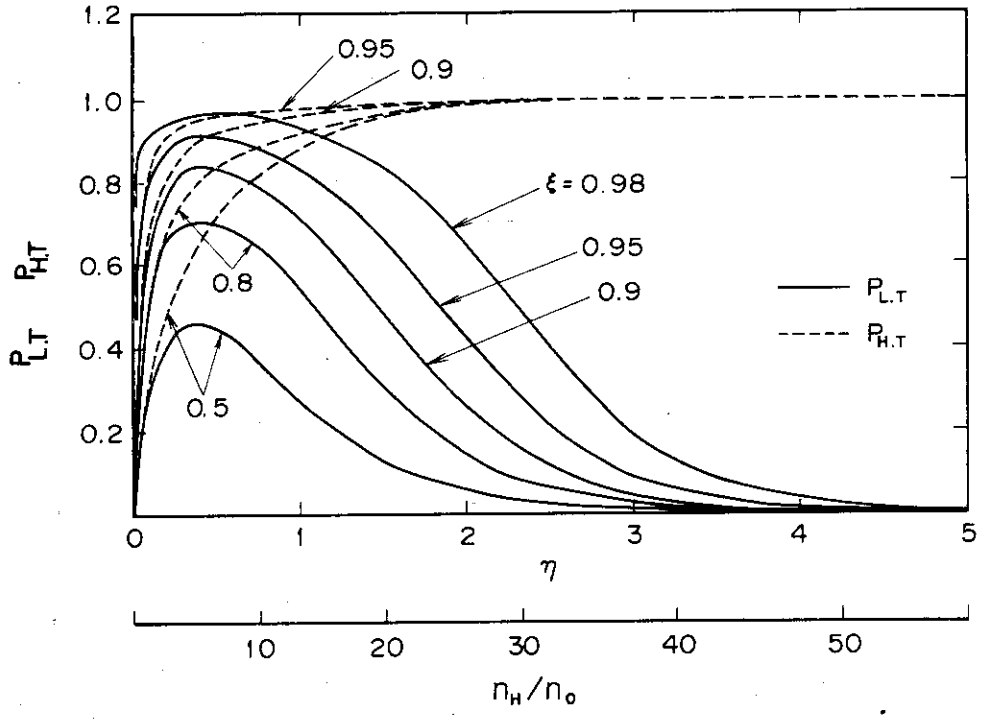

Fig. 6 Total power absorption of the incident wave from the higher magnetic field side $P_{H.T}$ and the lower magnetic field side $P_{L.T}$ after the infinity reflection with parameter ξ.

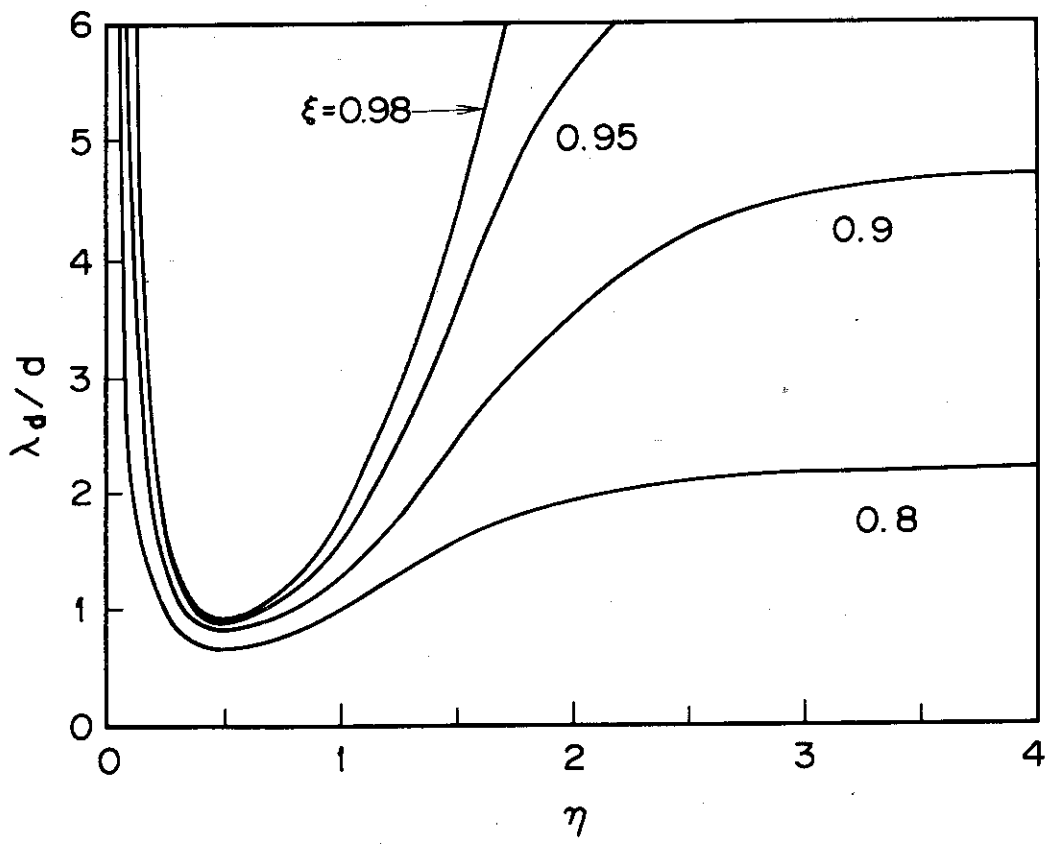

Fig. 7 Toroidal damping length of the incident wave from the lower magnetic field side with parameter ξ.

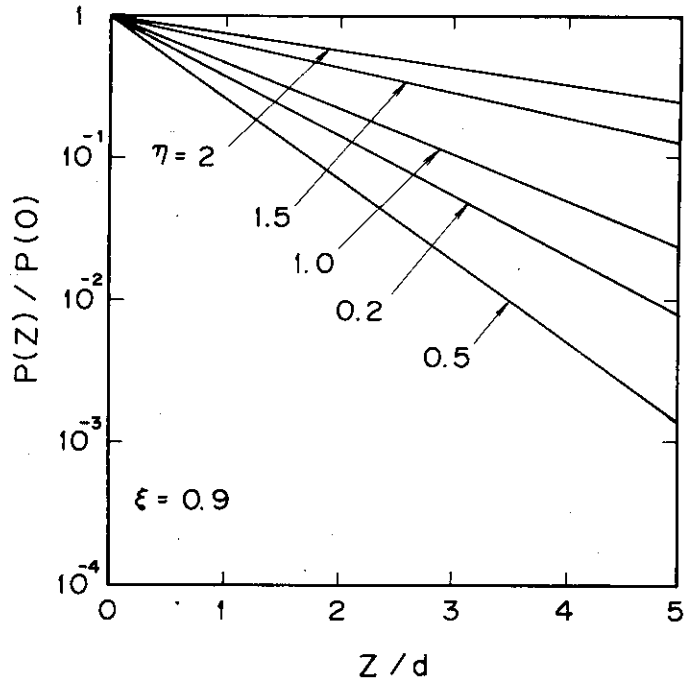

Fig. 8 Spatial evolution of the wave power incident from the lower magnetic field side with parameter η.

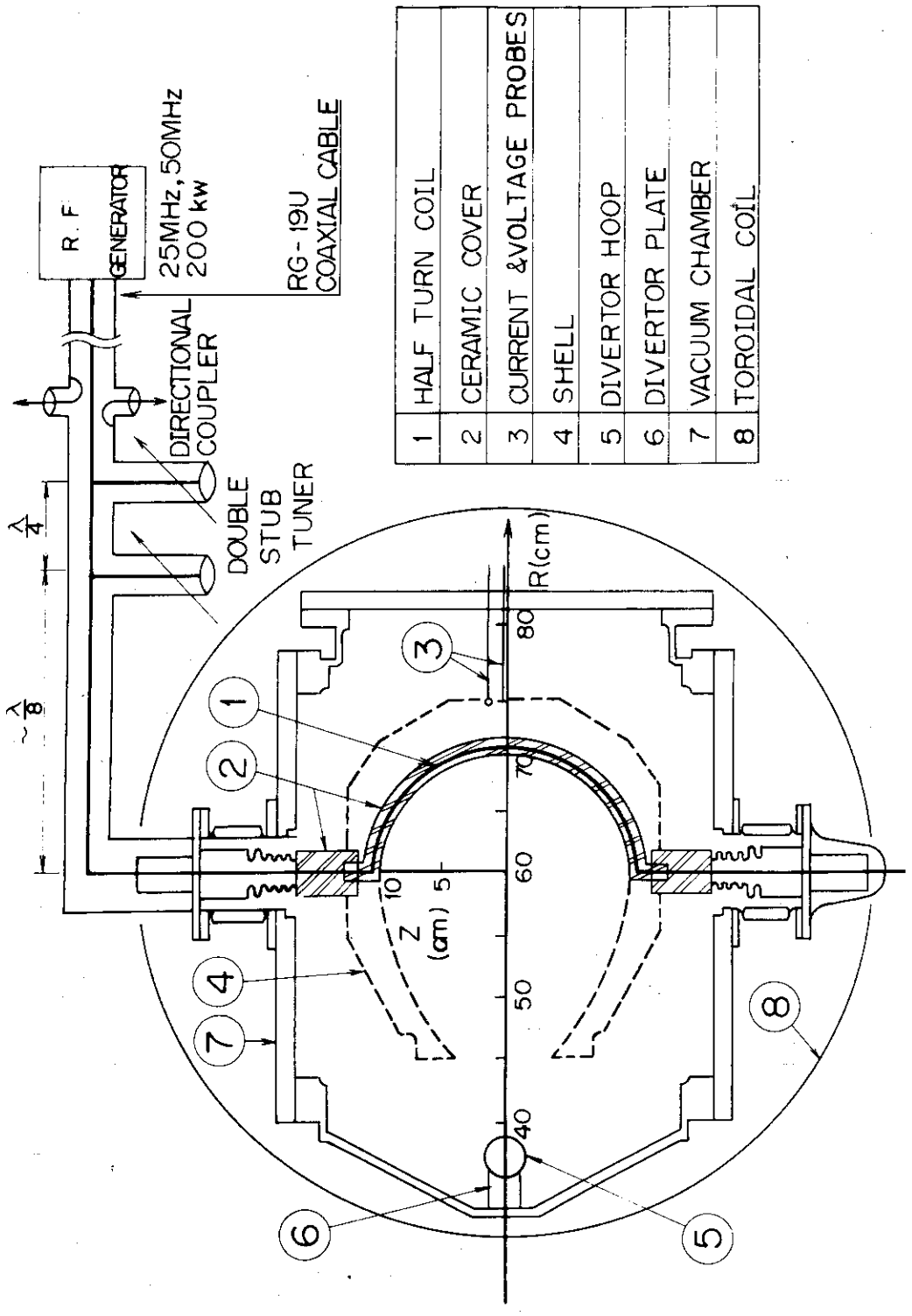

Fig. 9 Schematic view of the plasma cross section with rf launching system.

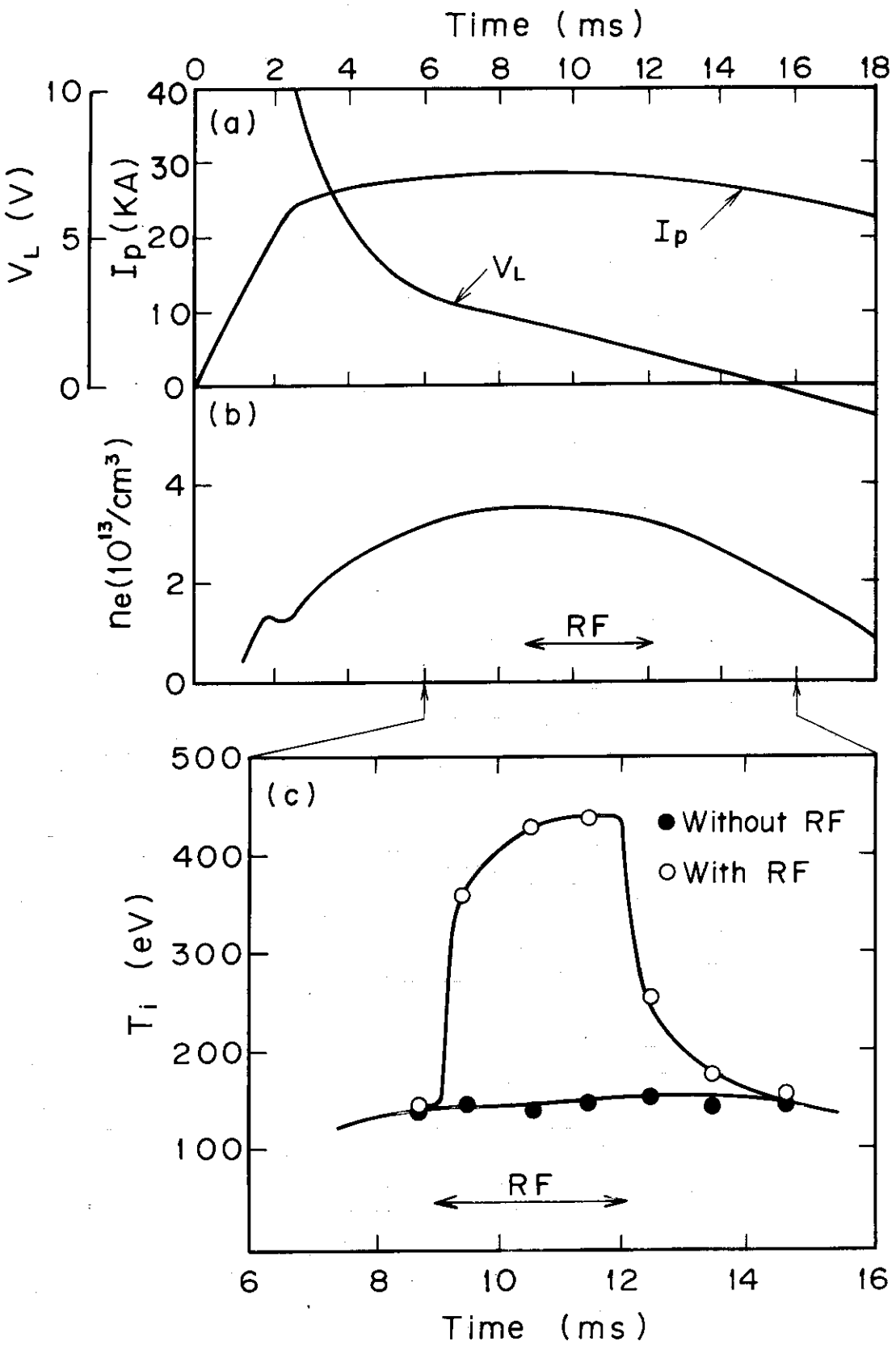

Fig.10 (a) Time evolution of the plasma current I_P, one turn loop voltage V_L and (b) the electron density n_e and (c) the ion temperature with and without rf power.

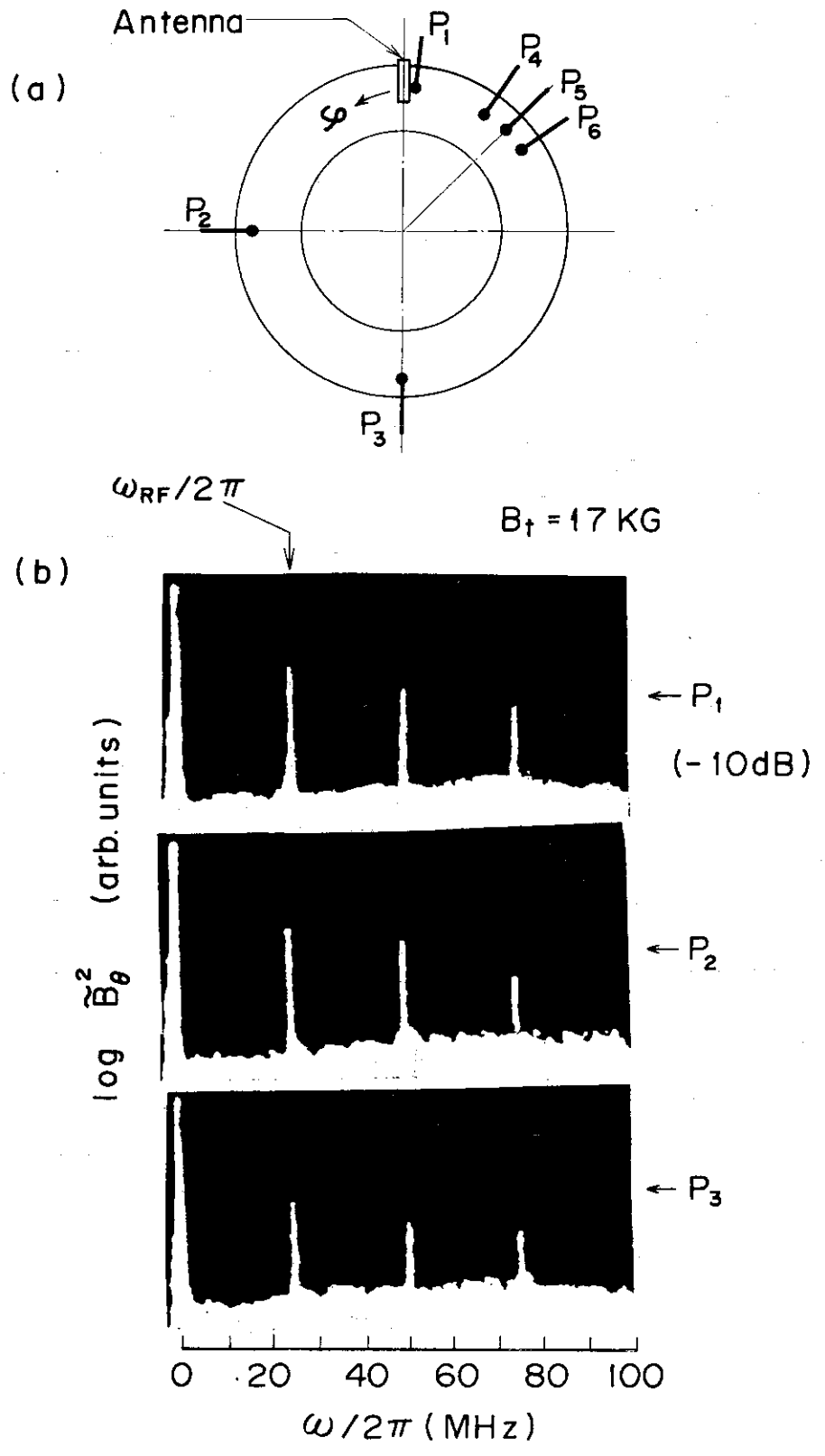

Fig.11 (a) Schematic drawing of the six probe positions in toroidal direction. (b) Detected power frequency spectrum measured by probe P_1, P_2 and P_3.

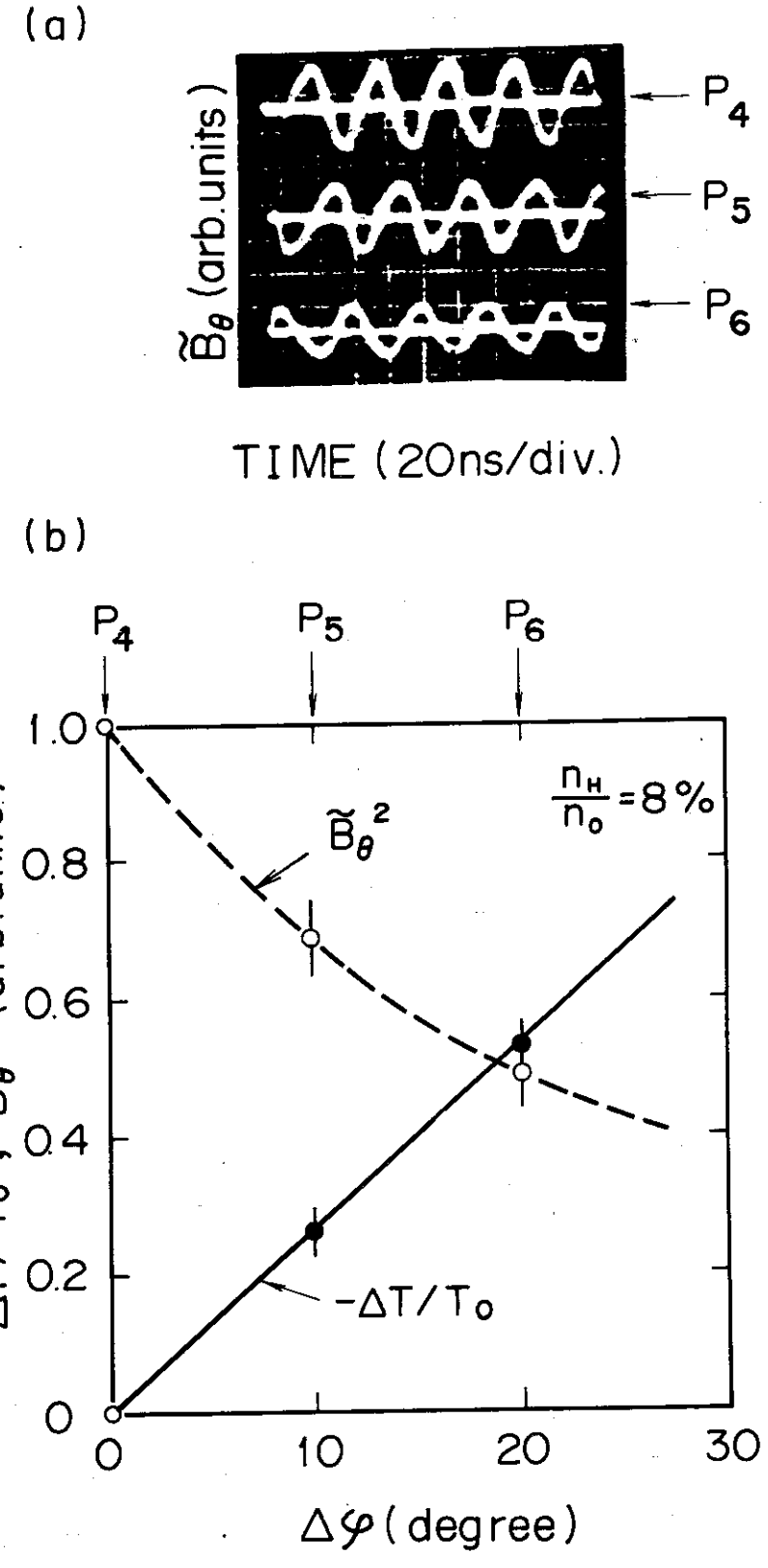

Fig.12 (a) Oscillogram of the three closed probes P_4, P_5 and P_6.
(b) Time delay normalized by a period and squared relative amplitude along the toroidal angle.

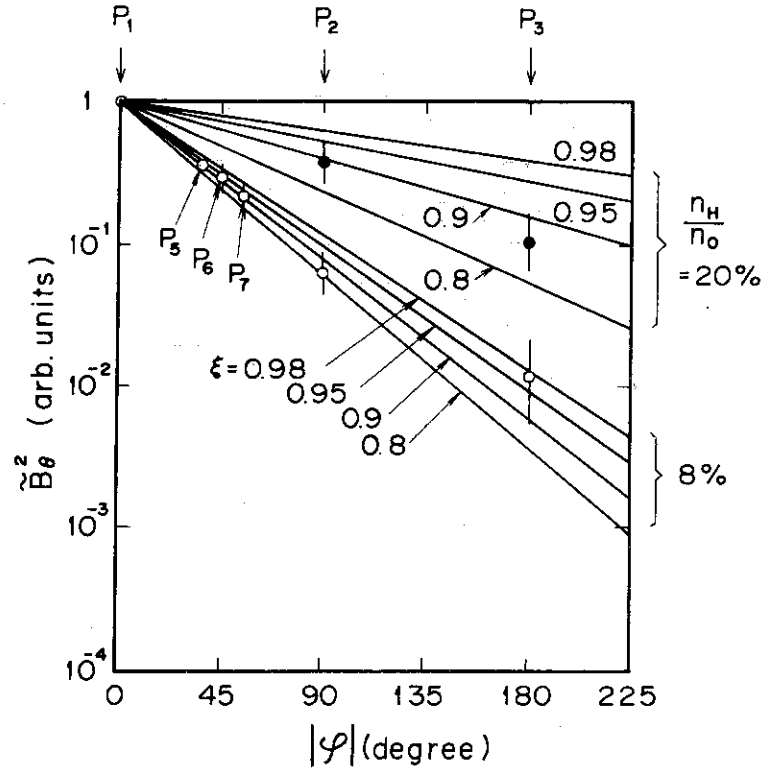

Fig.13 Spatial evolution of the detected power amplitude along the toroidal angle with parameter n_H/n_0 and ξ.

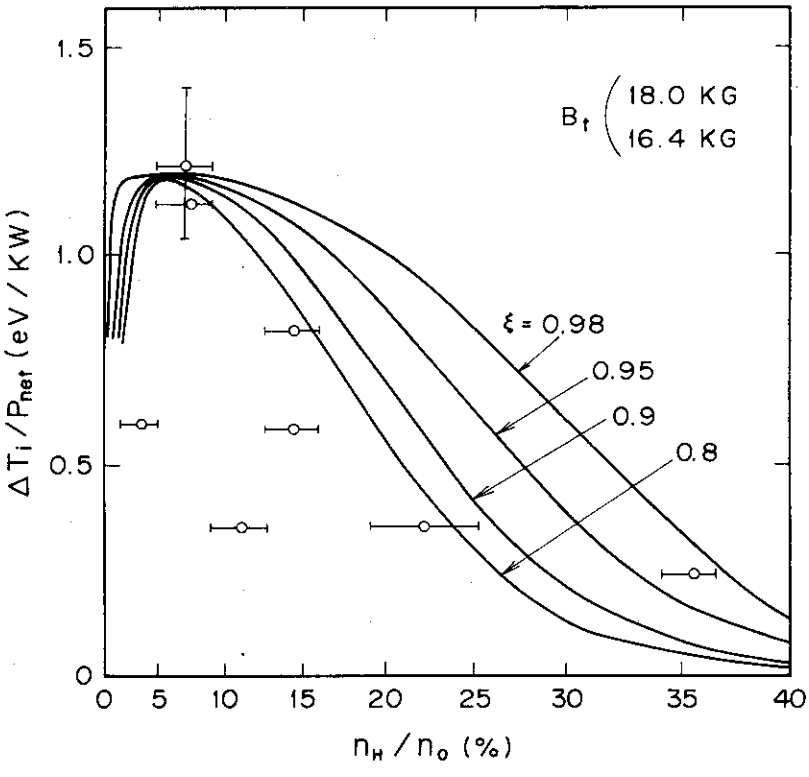

Fig.14 Increase of the ion temperature against to the ratio n_H/n_0. Theoretical curves are calculated with the parameter ξ.

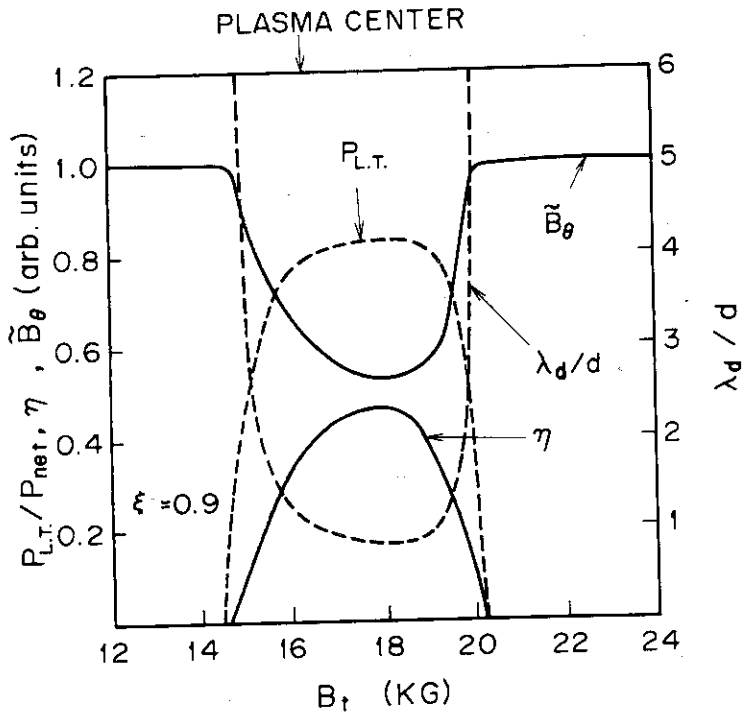

Fig.15 Theoretical dependences of η, damping length λ_d/d, the absorbed power $P_{L.T}$ and the relative amplitude $\tilde{B}_\theta$ on the strength of the toroidal magnetic field.

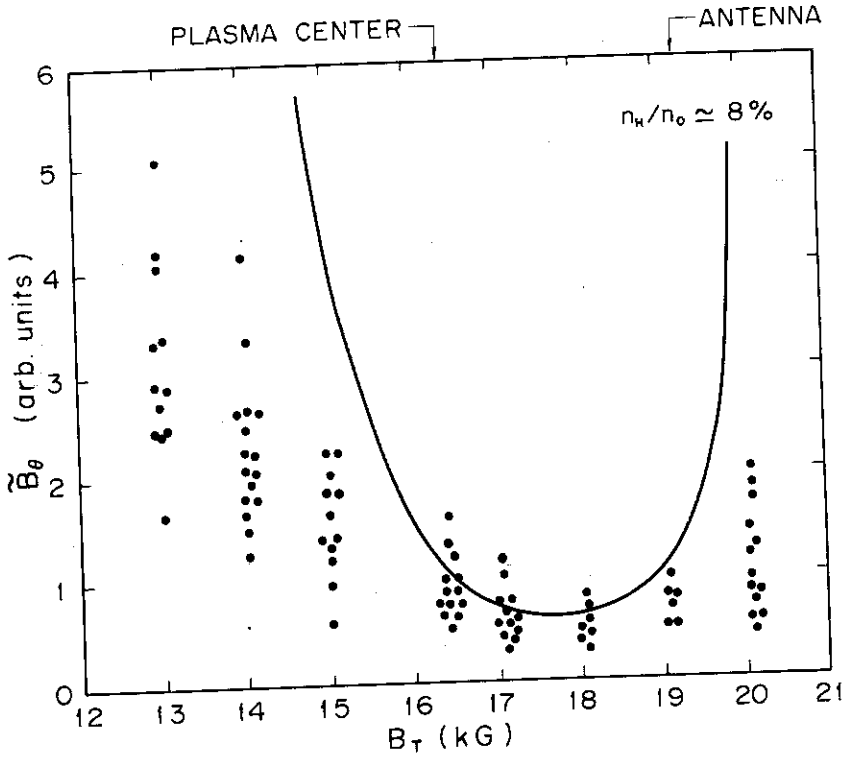

Fig.16 Observed wave amplitude of probe P_3 and the theoretical relative amplitude.

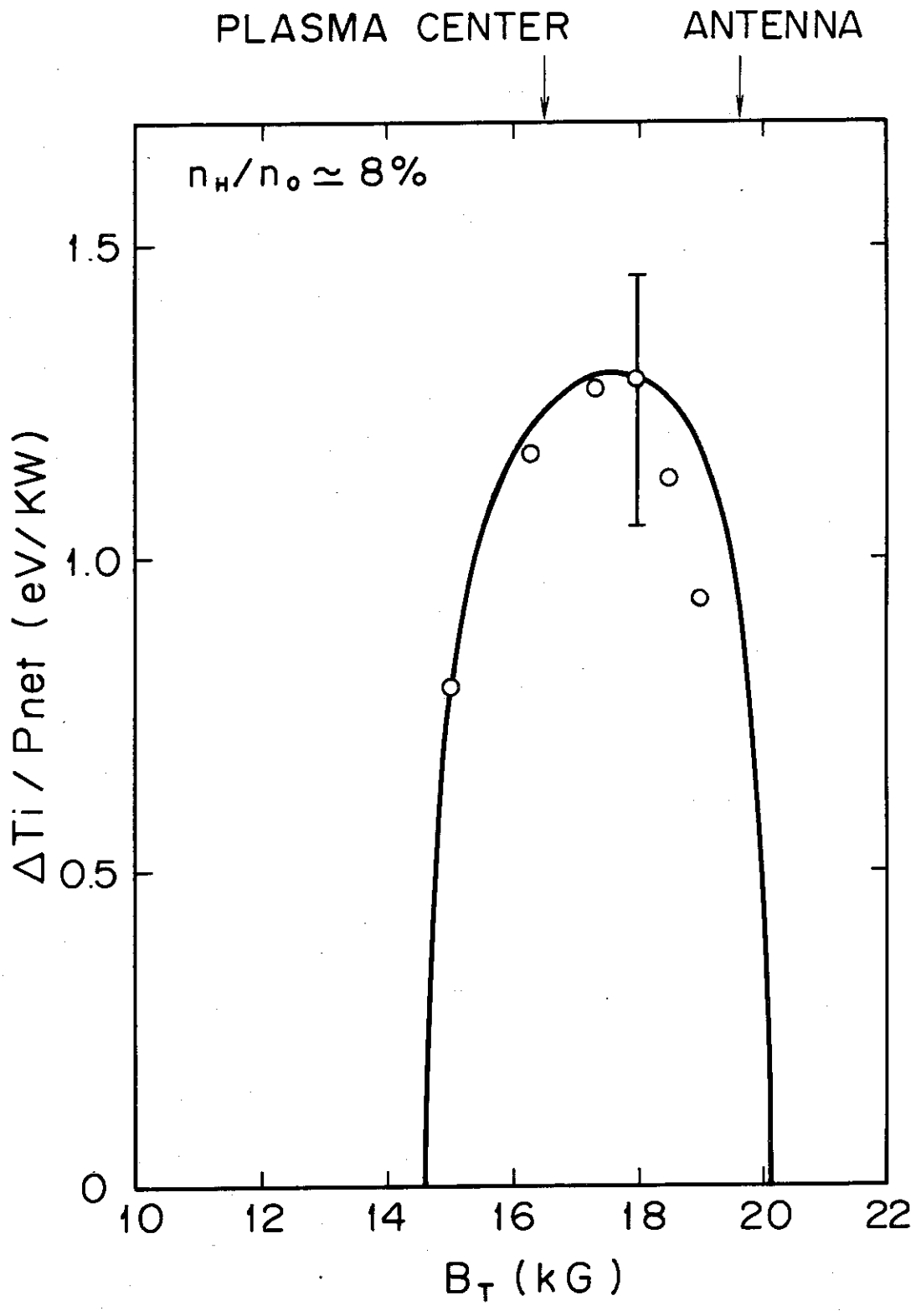

Fig.17 Increase of the ion temperature and the theoretical relative absorbed wave power.